Physics Letters B 770 (2017) 539–545

Contents lists available at ScienceDirect

Physics Letters B

www.elsevier.com/locate/physletb

Radiative distortion of kinematic edges in cascade decays

M. Beneke [a], L. Jenniches [b], A. Mück [c,*], M. Ubiali [d]

[a] Physik Department T31, James-Franck-Straße 1, Technische Universität München, D-85748 Garching, Germany
[b] Institut für Theoretische Physik und Astrophysik, Universität Würzburg, D-97074 Würzburg, Germany
[c] Institut für Theoretische Teilchenphysik und Kosmologie, RWTH Aachen University, D-52056 Aachen, Germany
[d] Cavendish Laboratory, HEP group, University of Cambridge, J.J. Thomson Avenue, Cambridge CB3 0HE, United Kingdom

ARTICLE INFO

Article history:
Received 13 December 2016
Accepted 11 April 2017
Available online 13 April 2017
Editor: A. Ringwald

ABSTRACT

Kinematic edges of cascade decays of new particles produced in high-energy collisions may provide important constraints on the involved particles' masses. For the exemplary case of gluino decay $\tilde{g} \to q\bar{q}\tilde{\chi}$ into a pair of quarks and a neutralino through a squark resonance, we study the hadronic invariant mass distribution in the vicinity of the kinematic edge. We perform a next-to-leading order calculation in the strong coupling α_s and the ratio of squark width and squark mass $\Gamma_{\tilde{q}}/m_{\tilde{q}}$, based on a systematic expansion in $\Gamma_{\tilde{q}}/m_{\tilde{q}}$. The separation into hard, collinear and soft contributions elucidates the process-dependent and universal features of distributions in the edge region, represented by on-shell decay matrix elements, universal jet functions and a soft function that depends on the resonance propagator and soft Wilson lines.

1. Introduction

The kinematics of particle decay leads to sharp edges in certain distributions, whenever the decay proceeds through another intermediate resonance. Well-known examples are the invariant mass of the lepton pair in squark decay $\tilde{q} \to q\ell^+\ell^-\tilde{\chi}$ through a neutralino and a slepton resonance [1,2], and the hadronic invariant mass distribution $d\Gamma/dM_h^2$ in gluino decay $\tilde{g} \to q\bar{q}\tilde{\chi}$ through a squark resonance (see diagrams in Fig. 1). The latter displays an edge at

$$M_{\text{edge}}^2 = \frac{(m_{\tilde{g}}^2 - m_{\tilde{q}}^2)(m_{\tilde{q}}^2 - m_{\tilde{\chi}}^2)}{m_{\tilde{q}}^2}\,. \tag{1}$$

The sharp feature provides a constraint on the supersymmetric particle masses involved in the decay. In practice, the edge will be smeared out by detector effects, the extent of which depends on the experimental set-up. However, even on purely theoretical grounds, the sharp edge is expected to be smoothed by radiative corrections and by the width of the intermediate resonance.

In order to predict the spectra locally near the kinematic edge the narrow-width approximation for the intermediate resonance cannot be applied. This is evident from the fact that the leading radiative correction contains a logarithmic singularity

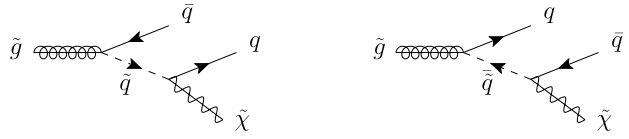

Fig. 1. Tree diagrams representing the gluino decay $\tilde{g} \to q\bar{q}\tilde{\chi}$ through an intermediate squark or antisquark resonance.

$$\frac{\alpha_s}{\pi} \ln^2 \frac{|M_h^2 - M_{\text{edge}}^2|}{M_{\text{edge}}^2}\,. \tag{2}$$

In the edge region, the distribution is sensitive to the resonance width $\Gamma_{\tilde{q}}$ even when $\Gamma_{\tilde{q}}/m_{\tilde{q}} \ll 1$ and contains potentially large logarithms $\ln m_{\tilde{q}}/\Gamma_{\tilde{q}}$.[1] A reliable theoretical framework must account for the presence of the scale $\Gamma_{\tilde{q}}$. Radiation and interference effects lead to a distortion of the distribution near the kinematic edge.

In this work we quantify this distortion. We define the edge region and study the factorization property of the hadronic invariant mass distribution at leading order in the expansion in the ratio $\Gamma_{\tilde{q}}/m_{\tilde{q}}$. The distribution is then computed at next-to-leading order (NLO) in the strong coupling α_s and leading order (LO) in $\Gamma_{\tilde{q}}/m_{\tilde{q}}$,

[1] The width of the resonance determines the extent of the edge region, see the following section, which decreases when the resonance is longer-lived. Incidentally, the singular logarithms were not observed in the next-to-leading order QCD calculation of the process $\tilde{q} \to q\ell^+\ell^-\tilde{\chi}$ in the narrow-width approximation [3], since the distribution was binned in bin sizes larger than the width.

* Corresponding author.
E-mail address: mueck@physik.rwth-aachen.de (A. Mück).

http://dx.doi.org/10.1016/j.physletb.2017.04.018

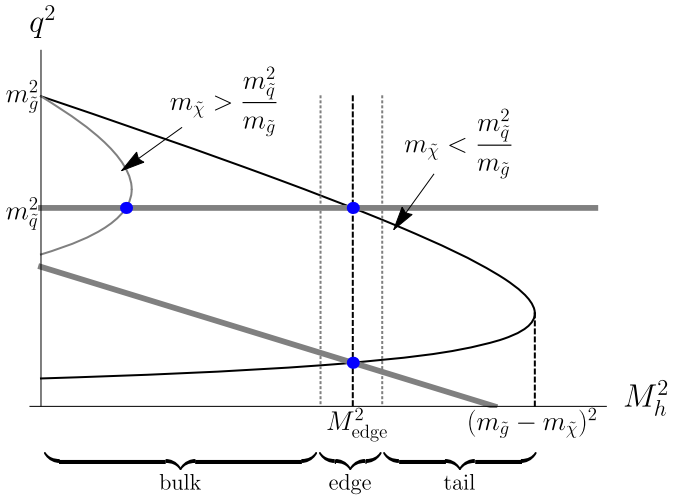

Fig. 2. Tree-level phase space in the squark momentum squared q^2 and the hadronic invariant mass squared M_h^2. For the case $m_{\tilde\chi} < m_{\tilde q}^2/m_{\tilde g}$ we show the bulk, edge and tail regions and the lines (in thick gray) where the (anti)squark is on-shell. The intersection of these lines with the phase-space boundary (dots) defines the edge invariant mass, which is shown also for the case $m_{\tilde\chi} > m_{\tilde q}^2/m_{\tilde g}$. The non-horizontal gray line corresponds (for the case $m_{\tilde\chi} < m_{\tilde q}^2/m_{\tilde g}$ only) to the resonant value of the second diagram in Fig. 1.

and at NLO in $\Gamma_{\tilde q}/m_{\tilde q}$ but LO in α_s. The resummation of logarithms of $\Gamma_{\tilde q}/m_{\tilde q}$ is left to future work. Our result therefore applies when $\Gamma_{\tilde q}/m_{\tilde q}$ is small, but not extremely small. We plan to present further details and results in a longer technical write-up [9].

2. The edge region

2.1. Kinematics

We consider the gluino decay chain $\tilde g \to \tilde q\,(\to q + \tilde\chi) + \bar q$ through an intermediate squark resonance into a neutralino. At tree level, the neutralino is accompanied by a quark–antiquark pair with invariant mass M_h. The edge value (1) is the maximal value the hadronic invariant mass can take for tree kinematics, when the squark momentum q is on-shell, $q^2 = m_{\tilde q}^2$. The tree-level phase space is shown in Fig. 2. The edge value naturally divides the hadronic invariant mass into three regions. The "edge region" is the strip of width $\mathcal{O}(\Gamma_{\tilde q})$, in which the squark propagator can remain resonant, but the distribution is sensitive to the precise virtuality of the propagator. Values $M_h > M_{\rm edge}$ up to $m_{\tilde g} - m_{\tilde\chi}$ are accessible only when the squark propagator is off-shell. We refer to this as the "tail region". The tree-level distribution falls off rapidly in this region. Finally, the region of hadronic invariant mass below the edge region is called the "bulk region". In this region the shape of the bulk of the invariant mass distribution is determined by the cascade of two decay processes through an intermediate on-shell squark.

The edge region is the only region that requires a special treatment, because it is intrinsically sensitive to the scale of the resonance width, which enters the resonance propagator. While in the bulk region the resonance is also on-shell, the propagator can still be expanded in the distribution sense, treating $\Gamma_{\tilde q}$ as small. At leading order in $\Gamma_{\tilde q}/m_{\tilde q}$, this amounts to the narrow-width approximation. In the tail region, on the other hand, the distribution is power-suppressed.

At tree level, invariant masses in the edge region can be produced in two ways. For resonant squarks the edge value is attained if the quark and antiquark are back-to-back, since the invariant mass increases with the angle θ between the quark and antiquark momenta. Alternatively, $M_{\rm edge}$ can also be achieved by $q^2 > m_{\tilde q}^2$ or $q^2 < m_{\tilde q}^2$, in which case $\cos\theta$ does not need to be -1. However, this contribution is power-suppressed due to the off-shell squark propagator. Whether q^2 must be larger or smaller than $m_{\tilde q}^2$ depends on whether the neutralino mass is larger or smaller than $m_{\tilde q}^2/m_{\tilde g}$. The value of the neutralino mass also determines the resonant decay kinematics in the edge region. For small $m_{\tilde\chi} < m_{\tilde q}^2/m_{\tilde g}$, the neutralino momentum is aligned with the antiquark momentum, otherwise with the quark momentum.

Since the gluino and neutralino are Majorana fermions, there is another decay chain, $\tilde g \to \bar{\tilde q}\ (\to \bar q + \tilde\chi) + q$, where the quark and antiquark momenta are interchanged and the resonance is an antisquark (see second diagram in Fig. 1), which interferes with the squark resonance chain. At LO in $\Gamma_{\tilde q}/m_{\tilde q}$, however, the two processes can be treated as independent and contribute the same amount. The reason for this is that the interference of the two amplitudes necessarily requires one of the squark propagators to be off-shell, and hence is $\Gamma_{\tilde q}/m_{\tilde q}$ suppressed. We therefore focus on the first decay chain.

2.2. Factorization and leading regions

When the squark width is set to zero the invariant mass distribution drops to zero discontinuously at the edge value, which is unphysical. Our aim is to describe the shape of this distribution correctly at leading order in $\Gamma_{\tilde q}/m_{\tilde q}$, including radiative corrections.

We already noted that the quark and antiquark must be nearly back-to-back at tree level. It is evident that tree-level kinematics is not changed, if a) the gluino and squark decay vertices are modified by hard-virtual corrections, b) the quark and antiquark develop into jets by collinear emissions, and c) soft gluons connect all strongly interacting particles in the squared amplitude. We therefore introduce the hard $(1,1,1)$, collinear $(1,\lambda,\sqrt{\lambda})$, anti-collinear $(\lambda,1,\sqrt{\lambda})$ and soft $(\lambda,\lambda,\lambda)$ regions, where $\lambda = \Gamma_{\tilde q}/m_{\tilde q}$.[2] Here, following soft-collinear effective theory (SCET) notation [4,5], we introduced two light-like vectors, $n_\pm^2 = 0$, and decomposed a four-vector into components $(n_+p, n_-p, p_\perp)$. The hard, soft, and jet functions and the interactions of these modes are familiar objects in SCET. In addition, the effective theory after integrating out hard modes includes a resonant mode that describes squarks with off-shellness of order λ, a situation that is described by unstable-particle effective theory [6]. The soft-collinear physics is reminiscent of event shapes in e^+e^- annihilation in the phase-space region of two-jet final states. However, in the edge region of the cascade decay the two jets do not emanate from a point-like vertex, but from two points, the production and the decay vertices of the long-lived resonance. As a consequence the soft physics is much more complicated.

We can therefore write down a factorization formula for the hadronic mass distribution of the form

$$\frac{d\Gamma}{dM_h^2} = |C|^2 \cdot |D|^2 \cdot J \otimes \bar J \otimes \big[R \otimes \bar R \otimes S\big] + HR\,, \tag{3}$$

which is valid in the vicinity of $M_{\rm edge}^2$, at leading power in $\Gamma_{\tilde q}/m_{\tilde q}$, and graphically presented in Fig. 3. The first two factors on the right-hand side of this equation consist of the square of two hard functions, one (C) containing the hard virtual correction to the on-shell gluino decay $\tilde g \to \tilde q + \bar q$, the other ($D$) to the on-shell squark decay $\tilde q \to q + \tilde\chi$. The hard functions multiply the (anti)quark jet functions J, $\bar J$, which contain the collinear (J) and anti-collinear

[2] We do not distinguish $m_{\tilde g}$ and $m_{\tilde q}$ for the purpose of power counting.

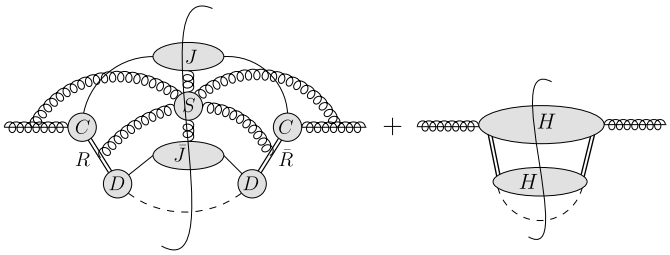

Fig. 3. Graphical representation of the factorization formula for the hadronic invariant mass distribution in the edge region.

($\bar{J}$) modes. These are convoluted with a soft function that consists of the resonant squark propagators R, $\bar{R}$ in unstable-particle effective theory, and a vacuum matrix element S of soft Wilson lines factored off the jets, the gluino, and the resonances. Due to the spatial separation of the two hard decay vertices, the soft function is a highly non-local object in position space, which accounts for the distribution of soft momentum between the various factors and for the distortion of the shape of the resonance.

The first term in (3) would be all there is, if requiring $M_h^2 \approx M_{\rm edge}^2$ *always* forced the hadronic final state to consist of two back-to-back jets. However, hard (i.e. non-collinear) real emission is also possible. While the interference of hard emission amplitudes *between* the two decay stages is power-suppressed, since at least one squark propagator is then thrown off resonance, interference *within* the two decay stages separately can leave the squarks on-shell. In terms of Feynman diagrams the hard parton final state can therefore be described as a cluster of partons with invariant mass p_J^2 emerging from the gluino decay vertex and another cluster with mass $p_{\bar{J}}^2$ from the squark decay vertex, replacing the antiquark and quark in the tree diagram, respectively, such that the total invariant mass is near $M_{\rm edge}^2$. Note that p_J^2 and $p_{\bar{J}}^2$ are now generically of $\mathcal{O}(1)$ while only the phase-space region when both are $\mathcal{O}(\lambda)$ is included in the first term on the right-hand side of (3). The additional hard-real contribution is denoted by HR in this equation and must be added by explicit matching. In practice, this amounts to the calculation of hard real radiation to the separate decay stages in dimensional regularization, setting the external squark line on-shell and M_h^2 to $M_{\rm edge}^2$. These simplifications automatically avoid double counting with the first term of (3) and correspond to the direct computation of the hard region according to the method-of-regions strategy [7].

An intuitive understanding of hard real radiation is obtained from looking at the maximal value of M_h^2 for on-shell squarks in the presence of hard radiation. If this value is larger than $M_{\rm edge}^2$, the previous edge value lies in the bulk region of the hard radiative process.[3] The latter therefore becomes insensitive to the width of the squark and can be treated like the bulk distribution at tree level. The HR term is therefore simply a constant contribution to $d\Gamma/dM_h^2$ in the edge region. The structure of (3) is similar to resonant and non-resonant production in the factorization formula for the line-shape of a resonance or pair production near threshold in previous applications of unstable-particle effective theory (see the review [8]). However, here both terms appear at leading power due to the presence of a resonant bulk region at tree-level rather than a single resonant invariant mass or threshold energy. Hence the non-resonant contribution is replaced by the resonant, but width-insensitive and unsuppressed hard-real contribution.

We shall provide a formal discussion of the factorization formula together with technical details in a separate paper [9].

3. NLO invariant mass distribution

At leading order, the factorization formula (3) becomes trivial. Without any additional gluon, there is no hard radiation. The soft and jet functions are unity. Defining the product of spin-averaged/spin-summed tree-level squared matrix elements $M^2(\hat{q}^2) = |M(\tilde{g} \to \tilde{q} + \bar{q})|^2 |M(\tilde{q} \to q + \tilde{\chi})|^2$, the hard functions are given by $M^2(0)$, i.e. for vanishing off-shellness $\hat{q}^2 = q^2 - m_{\tilde{q}}^2 = 0$ of the squark. Since the on-shell kinematics is completely fixed at tree level, $M^2(0)$ is constant in phase space. The resonance factor R is the propagator with a constant width $\Gamma_{\tilde{q}}$, so that R and $\bar{R}$ combine to a Breit–Wigner distribution. The integration of this distribution with respect to the off-shellness $\hat{q}^2$ of the squark is the only non-trivial phase-space integral. The measurement function for the hadronic mass introduces Θ-functions $\Theta\left(\hat{q}^2_{\rm max} - \hat{q}^2\right)$ and $\Theta\left(\hat{q}^2 - \hat{q}^2_{\rm min}\right)$, which determine the integration range. Depending on the sign of $\chi = (m_{\tilde{q}}^4 - m_{\tilde{g}}^2 m_{\tilde{\chi}}^2)/m_{\tilde{q}}^4$, either $\hat{q}^2_{\rm min}$ or $\hat{q}^2_{\rm max}$ is $\mathcal{O}(1)$, and the small off-shellness $\hat{q}^2$ can be neglected. Hence, the corresponding Θ-function is always equal to one and can be omitted. The integration boundary in the other Θ-function can be expanded to leading order in λ. Hence, the general result (3) simplifies to

$$\frac{d\Gamma_{\rm LO}}{dM_h^2} = \frac{M^2(0)}{256\pi^3 m_{\tilde{g}}^3} \int_{-\infty}^{\infty} d\hat{q}^2 \, \frac{\Theta\left(-\Delta - \hat{q}^2\chi\right)}{\hat{q}^4 + m_{\tilde{q}}^2\Gamma_{\tilde{q}}^2}\,, \tag{4}$$

where Δ is the $\mathcal{O}(\lambda)$ distance to the edge, i.e. $M_h^2 = M_{\rm edge}^2 + \Delta$. The Θ-function results in a universal tree-level shape of the edge distribution, since the dependence on the specific decay process appears only in the constant overall factor $M^2(0)$.

We remark that at leading power in $\Gamma_{\tilde{q}}/m_{\tilde{q}}$, the Θ-function in (4) is absent in the bulk region, since the second integration boundary is also $\mathcal{O}(1)$. Therefore, the differential width is constant in the bulk. In the tail region, on the other hand, the Θ-functions make the differential width vanish.

3.1. Next-to-leading power at tree level

Before turning to the calculation of the radiative corrections, we briefly discuss how the next term in the expansion in $\Gamma_{\tilde{q}}/m_{\tilde{q}}$ of the tree-level distribution is computed in the edge region. At $\mathcal{O}(\lambda)$, the numerator $M^2(\hat{q}^2)$ in (4) is not only needed for on-shell decays ($\hat{q}^2 = 0$) but one needs the next order in the Taylor-expansion of the off-shell matrix elements with respect to $\hat{q}^2$. Hence, one part of the resonant contribution is given by

$$\frac{d\Gamma_{\rm NLO}^{\rm res}}{dM_h^2} = \frac{dM^2(\hat{q}^2)/d\hat{q}^2|_{\hat{q}^2=0}}{256\pi^3 m_{\tilde{g}}^3} \times \int_{-\infty}^{\infty} d\hat{q}^2 \left(\frac{\hat{q}^2}{\mu^2}\right)^{\epsilon} \Theta\left(-\Delta - \hat{q}^2\chi\right) \frac{\hat{q}^2}{\hat{q}^4 + m_{\tilde{q}}^2\Gamma_{\tilde{q}}^2}\,, \tag{5}$$

where we have introduced the factor $\hat{q}^{2\epsilon}$ in order to make the integral well-defined. For $\chi > 0$, the previous expression evaluates to

[3] This criterion also implies that at the level of one-gluon emission the hard gluon must be emitted from squark decay for light neutralinos $m_{\tilde{\chi}} < m_{\tilde{q}}^2/m_{\tilde{g}}$, and from gluino decay for $m_{\tilde{\chi}} > m_{\tilde{q}}^2/m_{\tilde{g}}$.

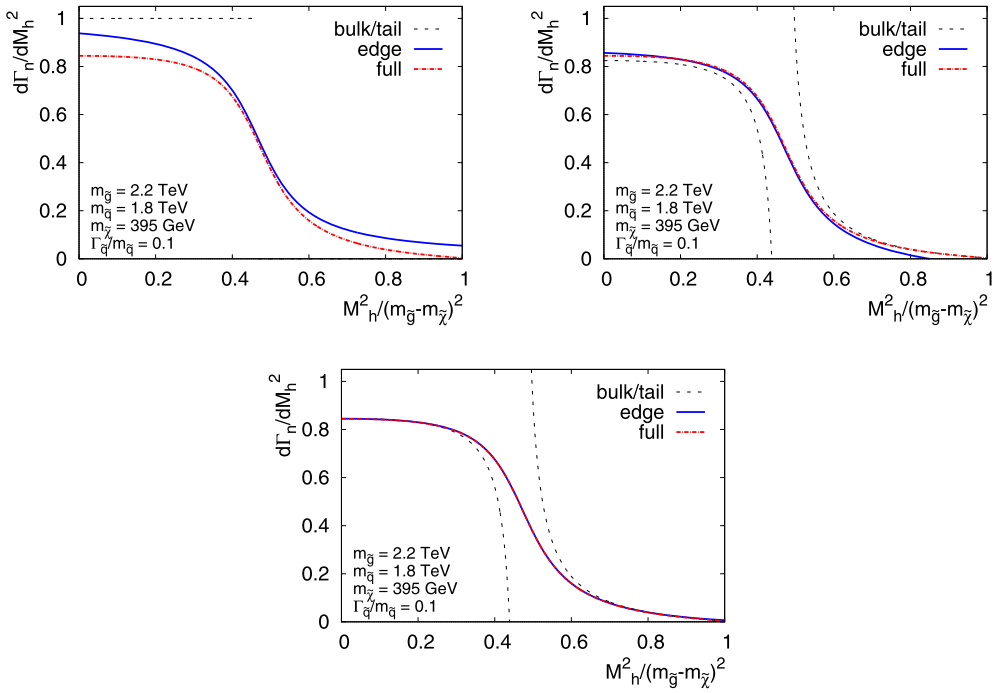

Fig. 4. Tree-level invariant mass spectrum for the SUSY benchmark point A with width $\Gamma_{\tilde{q}} = m_{\tilde{q}}/10$ discussed below. We normalize the differential width to the constant LO result in the bulk region. The blue solid line refers to the edge distribution, the black dashed line to the tail and bulk distribution, and the red dot-dashed line to the exact tree-level result in the fixed-width scheme. The interference contribution is not included. From left to right to bottom the leading power (left), next-to-leading power (right), and next-to-next-to-leading power (bottom) terms are successively included. (For interpretation of the references to color in this figure, the reader is referred to the web version of this article.)

$$\frac{d\Gamma^{\rm res}_{\rm NLO}}{dM_h^2} = \frac{dM^2(\hat{q}^2)/d\hat{q}^2|_{\hat{q}^2=0}}{256\pi^3 m_{\tilde{g}}^3} \times \left[\frac{1}{\epsilon} + i\pi + \frac{1}{2}\ln\left(\frac{m_{\tilde{q}}^2\Gamma_{\tilde{q}}^2 + \Delta^2/\chi^2}{\mu^4}\right)\right], \tag{6}$$

where the $1/\epsilon$ pole and the spurious imaginary part are a consequence of factorizing the NLO contribution into a resonant and a non-resonant part, and of the choice of the regulating factor. Further, also the relevant integration boundary $\hat{q}^2_{\rm max}$ or $\hat{q}^2_{\rm min}$ discussed in the context of (4) receives an $\mathcal{O}(\lambda)$ correction, which can be taken into account by appropriately expanding the Θ-function. In addition, non-resonant contributions (with $|\hat{q}^2| \gg m_{\tilde{q}}\Gamma_{\tilde{q}}$) start to contribute at NLO. Here, the Breit–Wigner propagator can be expanded in the small width, and the Θ-function with respect to the small integration boundary. On the other hand, the second integration boundary can no longer be taken to infinity, and one also needs the full $\hat{q}^2$-dependence of the matrix elements. Hence, for $\chi > 0$ one finds

$$\frac{d\Gamma^{\rm non\text{-}res}_{\rm NLO}}{dM_h^2} = \frac{1}{256\pi^3 m_{\tilde{g}}^3}\int_{\hat{q}^2_{\rm min}}^{0} d\hat{q}^2 \left(\frac{\hat{q}^2}{\mu^2}\right)^{\epsilon} \frac{M^2(\hat{q}^2)}{\hat{q}^4}, \tag{7}$$

where we consistently applied the same regulating factor $\hat{q}^{2\epsilon}$ as above to render the integral well-defined, and $\hat{q}^2_{\rm min}$ is calculated for $M_h^2 = M^2_{\rm edge}$. Since $M^2(\hat{q}^2)$ is polynomial in $\hat{q}^2$ in our case, the integral can be easily computed. Combining the resonant and the non-resonant contribution, the $1/\epsilon$ poles and spurious imaginary parts contained in (5) and (7) cancel and the regulator can be set to zero.

In the tail and in the bulk regions, the non-resonant contribution is integrated from $\hat{q}^2_{\rm min}$ to $\hat{q}^2_{\rm max}$, where $\hat{q}^2_{\rm max/min}$ is determined as a function of M_h^2. In the bulk, there is also a resonant contribution given by (5) without the Θ-function. In all three regions, higher-order contributions in $\Gamma_{\tilde{q}}/m_{\tilde{q}}$ are obtained in a straightforward way by expanding the relevant quantities (matrix elements, Θ-functions, Breit–Wigner propagators) to the appropriate order.

For the specific SUSY process under consideration the interference between the diagrams in Fig. 1 starts to contribute at NLO in $\Gamma_{\tilde{q}}/m_{\tilde{q}}$. There are two resonant contributions, where either the squark or the antisquark propagator is resonant and the other is off-shell, and quantities of $\mathcal{O}(\lambda)$ can be neglected in the remaining matrix element. There is also a non-resonant contribution, where $\hat{q}^2$ is considered to be large and the width can be neglected in both propagators.

In Fig. 4, we show numerical results for the tree-level hadronic invariant mass distribution at leading, next-to-leading, and next-to-next-to-leading power in $\Gamma_{\tilde{q}}/m_{\tilde{q}}$ for the SUSY benchmark point A discussed below, and compare them to the exact tree-level result. Rapid convergence upon including higher powers in $\Gamma_{\tilde{q}}/m_{\tilde{q}}$ can be observed.

3.2. Radiative correction

At next-to-leading order in the strong coupling α_s, an additional gluon line is attached in all possible ways to the square of the tree diagrams shown in Fig. 1. Hard virtual contributions amount to the evaluation of virtual corrections to each of the two two-body decays with an on-shell squark. They are also part of a standard narrow-width calculation [10] and we do not discuss them further here. In (3) they give the NLO corrections to the hard functions C and D, or equivalently the squared matrix elements $M^2(0)$ in (4). In addition, there are soft, collinear and hard-real corrections which correspond to the expansion of the soft function and the jet functions, and to the evaluation of the

hard real contribution in (3), respectively. They are discussed below.

All the individual pieces are in general separately divergent. When a soft gluon momentum r flows through a squark propagator with momentum k it is convenient to separate the UV divergent piece by adding and subtracting a term, such that the UV divergent term does not depend on the width and on $\hat{q}^2 = k^2 - m_{\tilde{q}}^2$:

$$\begin{aligned}\frac{1}{(k+r)^2 - m_{\tilde{q}}^2 + i m_{\tilde{q}}^2 \Gamma_{\tilde{q}}^2} &\stackrel{\mathcal{O}(\lambda)}{=} \frac{1}{\hat{q}^2 + 2\hat{k}\cdot r + i m_{\tilde{q}}^2 \Gamma_{\tilde{q}}^2} \\ &= \underbrace{\frac{1}{2\hat{k}\cdot r}}_{\text{soft UV}} + \underbrace{\frac{1}{\hat{q}^2 + 2\hat{k}\cdot r + i m_{\tilde{q}}^2 \Gamma_{\tilde{q}}^2} - \frac{1}{2\hat{k}\cdot r}}_{\text{soft remainder}}, \end{aligned} \tag{8}$$

where in the first step only terms of $\mathcal{O}(\lambda)$ are kept in the denominator. Hence, one can neglect the gluon momentum in the off-shellness $\hat{q}^2$, and set the squark momentum to its value $\hat{k}$ in the on-shell $1 \to 2$ gluino decay. In the following we separate the soft contributions into a term denoted "soft UV", which is simple and contains the UV divergence, and a finite "soft remainder" according to the above equation. If no soft gluon momentum flows through a squark propagator, the complete diagram is included in the soft UV contribution.

For collinear gluon exchange the complete matrix elements in the collinear approximation factor into the tree-level result and the appropriate splitting function. After integration, the collinear contributions correspond to the convolution of the jet function in (3) with the resonant squark propagator.

For soft and collinear gluon exchange the $\hat{q}^2$-integral in (4) has to be supplemented by a convolution with the gluon momentum. The virtual soft UV and collinear contributions are scaleless. For the real-emission soft UV and collinear contributions, the convolution can be cast into the standard form

$$\begin{aligned} B(\Delta, n, c) = \left(\frac{\mu}{\Gamma_{\tilde{q}}}\right)^{n\epsilon} &\int_0^\infty dy\, y^{-1-n\epsilon} \\ &\times \int_{-\infty}^{\infty} d\hat{q}^2\, \frac{\Theta(-\Delta - c\, y\, \Gamma_{\tilde{q}} m_{\tilde{q}}\, \chi - \hat{q}^2 \chi)}{\hat{q}^4 + m_{\tilde{q}}^2 \Gamma_{\tilde{q}}^2}, \end{aligned} \tag{9}$$

where μ is the scale from dimensional regularization and y is related to the small components of the soft or collinear gluon momenta. Since y enters the Θ-function at NLO for real gluon emission, the integral is not scaleless. In the bulk and in the tail regions, the argument of the Θ-function is $\mathcal{O}(1)$ and y must be neglected at leading power. Hence, in these regions there are no soft and no collinear contributions, as expected. The integral is given by

$$\begin{aligned} B(\Delta, n, c) &= -\frac{\mathrm{sgn}(\chi)}{m_{\tilde{q}}\Gamma_{\tilde{q}}}\, \Gamma(n\epsilon)\Gamma(-n\epsilon)\, \mathrm{Im}\left[x^{-n\epsilon}\right] \\ &= -\frac{\mathrm{sgn}(\chi)}{m_{\tilde{q}}\Gamma_{\tilde{q}}}\, \arg(x)\left(\frac{1}{n\epsilon} - \ln|x| \right. \\ &\quad \left. - \frac{n\epsilon}{6}\left(\arg^2(x) - \pi^2 - 3\ln^2|x|\right)\right) + \mathcal{O}(\epsilon^2), \end{aligned} \tag{10}$$

where $x = \frac{\Gamma_{\tilde{q}}}{\mu}\, \frac{\Delta/\chi + i m_{\tilde{q}}\Gamma_{\tilde{q}}}{c\, m_{\tilde{q}}\Gamma_{\tilde{q}}}$. The combined soft UV and collinear contribution to the differential width reads

$$\begin{aligned} \frac{d\Gamma_{\text{soft UV+coll}}}{dM_h^2} &= \frac{M^2(0)}{256\pi^3 m_{\tilde{g}}^3}\, \frac{\alpha_s}{\pi}\, e^{\gamma_E \epsilon} \\ &\quad \times \Big[B(\Delta, 2, c_i) A_i^{\text{soft UV}} + B(\Delta, 2, -c_f) A_f^{\text{soft UV}} \\ &\quad + B(\Delta, 1, c_i) A_i^{\text{coll}} + B(\Delta, 1, -c_f) A_f^{\text{coll}} \Big], \end{aligned} \tag{11}$$

where $c_i = m_{\tilde{q}}/m_{\tilde{g}}$, $c_f = m_{\tilde{g}}/m_{\tilde{q}}$, $\alpha_s = \alpha_s(\mu)$, and

$$\begin{aligned} A_i^{\text{soft UV}} &= C_{\tilde{g}\tilde{q}}\, \Gamma(\epsilon) - C_{\tilde{g}\tilde{g}}\, \Gamma(1+\epsilon) \\ &\quad - C_{\tilde{g}\tilde{q}}\, \Gamma(\epsilon) \frac{m_{\tilde{g}}^2 + m_{\tilde{q}}^2}{m_{\tilde{g}}^2 - m_{\tilde{q}}^2} \left[1 - \left(\frac{m_{\tilde{g}}^2}{m_{\tilde{q}}^2}\right)^{\epsilon}\right] \\ &\quad + C_{\tilde{q}\tilde{q}}\, \Gamma(\epsilon) \left(\frac{m_{\tilde{g}}^2}{m_{\tilde{q}}^2}\right)^{\epsilon} - C_{\tilde{q}\tilde{q}}\, \Gamma(1+\epsilon) \left(\frac{m_{\tilde{g}}^2}{m_{\tilde{q}}^2}\right)^{\epsilon}, \end{aligned} \tag{12}$$

$$A_f^{\text{soft UV}} = C_{\tilde{q}q}\, \Gamma(\epsilon) \left(\frac{m_{\tilde{q}}^2}{m_{\tilde{g}}^2}\right)^{\epsilon} - C_{\tilde{q}\tilde{q}}\, \Gamma(1+\epsilon) \left(\frac{m_{\tilde{q}}^2}{m_{\tilde{g}}^2}\right)^{\epsilon}, \tag{13}$$

$$\begin{aligned} A_i^{\text{coll}} &= C_F \left(\frac{\mu}{m_{\tilde{g}}}\right)^{\epsilon} \left(\frac{m_{\tilde{g}}^2 - m_{\tilde{q}}^2}{m_{\tilde{g}}^2}\right)^{-\epsilon} \frac{\Gamma(2-\epsilon)}{\Gamma(1-\epsilon)} \\ &\quad \times \left(\frac{\Gamma(-\epsilon)}{\Gamma(2-2\epsilon)} + \frac{\Gamma(2-\epsilon)}{2\Gamma(3-2\epsilon)}\right), \end{aligned} \tag{14}$$

$$\begin{aligned} A_f^{\text{coll}} &= C_F \left(\frac{\mu}{m_{\tilde{g}}}\right)^{\epsilon} \left(\frac{m_{\tilde{q}}^2 - m_{\tilde{\chi}}}{m_{\tilde{q}}^2}\right)^{-\epsilon} \frac{\Gamma(2-\epsilon)}{\Gamma(1-\epsilon)} \\ &\quad \times \left(\frac{\Gamma(-\epsilon)}{\Gamma(2-2\epsilon)} + \frac{\Gamma(2-\epsilon)}{2\Gamma(3-2\epsilon)}\right). \end{aligned} \tag{15}$$

Here the C_{ij} correspond to the color factors of the diagram with the gluon attached to i and j. To be specific $C_{\tilde{g}\tilde{g}} = N_c$, $C_{\tilde{g}\tilde{q}} = C_{\tilde{g}\bar{q}} = C_{\bar{g}q} = N_c/2$, $C_{\bar{q}\bar{q}} = C_{qq} = C_{\bar{q}q} = C_{\bar{q}\bar{q}} = C_F$, $C_{\bar{q}\tilde{q}} = C_{\bar{q}q} = C_F - N_c/2$ and in turn $C_F = 4/3$, $N_c = 3$. The different factors for the individual soft UV pieces are due to the angular integrals over the soft UV propagators. In the collinear case the Γ-functions are due to the integral over the collinear momentum fraction of the emitted gluon.

The coefficients in (12)–(15) contain $1/\epsilon$ poles which combine with the pole in (10) to cancel the poles of the hard virtual and hard real contributions. The above results are obtained with a $(4-2\epsilon)$-dimensional phase space for the gluon but with a 4-dimensional phase-space for the particles present at tree-level. We have verified that the final result, including the hard contributions calculated using the same convention, agrees with the result in conventional dimensional regularization.

The leading logarithmically enhanced corrections of the form $\ln^n(m_{\tilde{q}}/\Gamma_{\tilde{q}})$ $(n \le 2)$ in the full result can be extracted from (11) alone using the ϵ-expansion in (10). If μ is chosen $\mathcal{O}(m_{\tilde{q}})$, e.g. $\mu = m_{\tilde{q}}$, all large logarithms are contained in the soft UV + collinear part, since then the hard pieces depend only on $\mathcal{O}(1)$ ratios of dimensionful parameters. The soft remainder discussed below also does not contain large logarithms since it is finite, μ-independent, and homogeneous in the soft scale.

Due to the appearance of the width and $\hat{q}^2$ in the squark propagator, the virtual soft-remainder contributions are not scaleless. We evaluate the virtual diagrams by taking residues to convert them into phase-space diagrams. They then combine with the soft remainder from the real diagrams such that most infrared divergences cancel. Some diagrams, however, show a purely imaginary pole in the remainder which vanishes after adding the complex conjugate diagram.

The finite soft remainder contribution can be expressed in terms of a one-dimensional integral representation based on a single standard integral, i.e.

$$\begin{aligned}\frac{d\Gamma_{\text{soft remainder}}}{dM_h^2} &= \frac{M^2(0)}{256\pi^3 m_{\tilde g}^3}\frac{\alpha_s}{4\pi}\,\text{sgn}(\chi)\int_{-1}^{1}\text{d}x \\ &\times\Bigg[\left(\frac{C_{\tilde g\tilde q}}{\alpha}\,\frac{m_{\tilde g}^2+m_{\tilde q}^2}{2m_{\tilde g}^2}+\frac{C_{\tilde q\tilde q}-C_{\tilde q q}}{(1-x)\,\alpha}\right)F\left(\Delta,\frac{(1-x)\,c_i\,m_{\tilde q}}{\alpha\,m_{\tilde g}}\right) \\ &+\left(\frac{C_{\tilde q q}-C_{\tilde q q}}{(1+x)\,\alpha}\,\frac{m_{\tilde q}^2}{m_{\tilde g}^2}-\frac{C_{\tilde g q}}{1+x}-\frac{C_{\tilde q\tilde q}}{\alpha^2}\,\frac{m_{\tilde q}^2}{m_{\tilde g}^2}\right) \\ &\times F\left(\Delta,\frac{(1+x)\,c_f\,m_{\tilde q}}{\alpha\,m_{\tilde g}}\right)+\text{c.c.}\Bigg],\end{aligned}\tag{16}$$

where $\alpha=((1+x)m_{\tilde g}^2+(1-x)m_{\tilde q}^2)/(2m_{\tilde g}^2)$ and

$$F(\Delta,c)=I_+(\Delta,c-2)-I_+(\Delta,-2)-I_-(\Delta,c)\tag{17}$$

with

$$I_\pm(\Delta,\beta)=\frac{1}{im_{\tilde q}\Gamma_{\tilde q}}\left[\frac{\pi^2}{6}-\text{Li}_2\left(1+\beta\frac{i\,m_{\tilde q}\Gamma_{\tilde q}}{-\Delta/\chi\pm i\,m_{\tilde q}\Gamma_{\tilde q}}\right)\right].\tag{18}$$

In particular, diagrams where the gluon connects the gluino or the antiquark to the quark from squark decay only consist of these finite contributions.

Taking residues to evaluate the virtual loop diagrams, there are so-called particle-pole contributions (poles not due to the gluon propagator) which need additional analytic regularization to render separate soft and Glauber regions well-defined. All particle pole contributions vanish when properly regularized.

The hard real gluon emission contributes to the second term in (3). For hard gluon momenta, there is no non-trivial convolution between the squark and the gluon momentum, since $\hat q^2$ can be neglected in the argument of the measurement function, which is $\mathcal{O}(1)$ for a hard real gluon. For the same reason Δ can be neglected, and the resulting $d\Gamma_{\text{hard real}}/dM_h^2$ is a constant in the edge region. To compute HR, one has to compute the phase-space integral over the real-emission matrix elements for on-shell squarks as in a standard narrow-width calculation. Only the gluino (large $m_{\tilde\chi}$, $\chi<0$) or the squark decay (small $m_{\tilde\chi}$, $\chi>0$) contribute depending on the sign of χ, since the measurement function restricts the possible values for the quark–gluon and antiquark–gluon invariant masses for $M_h^2=M_{\text{edge}}^2$. It is convenient to use the following subtraction procedure. As usual the differential width is written as a phase-space integral over the squared matrix element involving the measurement function. We add and subtract the full squared matrix element divided by M_{edge}^2 without applying the measurement function, i.e.

$$\begin{aligned}|M|^2\delta(M_{\text{edge}}^2-M_h^2)&=\Big(|M|^2\delta(M_{\text{edge}}^2-M_h^2)-|M|^2/M_{\text{edge}}^2\Big)\\&\quad+|M|^2/M_{\text{edge}}^2\,.\end{aligned}\tag{19}$$

We first perform the phase-space integral over the angle between the quark and the antiquark. While the subtraction term is independent of this angle and can be trivially integrated, using the δ-function to perform the angle integral leads to non-trivial phase-space boundaries and a phase-space dependent factor multiplying the matrix element. In the soft-collinear phase-space region, which is always contained in the integration range, this factor tends to $1/M_{\text{edge}}^2$. Hence, the remaining phase-space integration over the subtracted piece in parenthesis in (19) is finite in four dimensions and can be easily computed (we use a one-dimensional integral representation for our numerical results). The remaining term in (19) is proportional to the real-emission contribution to the total width upon integration. It has to be calculated using dimensional regularization but it is known from inclusive narrow-width calculations.

The hard virtual, the hard real, and the soft UV and collinear contributions in (11) individually include poles in $1/\epsilon$. In contrast to an inclusive calculation, the poles in the hard virtual and hard real pieces do not cancel at the edge because of the non-trivial $\hat q^2$ integral (4), which multiplies the hard virtual correction. Together with the soft and collinear contributions in (11), the differential width is, of course, finite (diagram by diagram if the collinear contributions are split accordingly). The sum of the hard virtual and hard real corrections for the inclusive calculation agrees with the results in [10].

The choice of SUSY benchmark points for our numerical analysis is based on the exclusion limits in terms of simplified models provided by ATLAS [11]. We analyzed two points which are not excluded, one for $\chi>0$ and one $\chi<0$, with parameters

- benchmark A: $m_{\tilde g}=2.2$ TeV, $m_{\tilde q}=1.8$ TeV, $m_{\tilde\chi}=395$ GeV, $\chi>0$
- benchmark B: $m_{\tilde g}=2.2$ TeV, $m_{\tilde q}=1.0$ TeV, $m_{\tilde\chi}=695$ GeV, $\chi<0$

Note that all results depend only on the ratios of the masses and the squark width. We use the squark width as a free parameter to investigate the edge behavior for different values of $\Gamma_{\tilde q}/m_{\tilde q}$. For the renormalization scale we use $\mu=m_{\tilde g}$ with $\alpha_s(\mu)=0.0799$. In Fig. 5 we show the result for benchmark A. The scenario B exhibits similar features and is therefore not shown. The figures display the full LO result in α_s (including all power corrections) for the hadronic invariant mass distribution $d\Gamma_{\text{LO}}/dM_h^2$ (black dashed). To this we add the NLO QCD corrections at leading power $\Gamma_{\tilde q}/m_{\tilde q}$ in the edge region (red solid), which is our main result, and the NLO QCD corrections in the narrow-width approximation in the bulk and in the tail region, which diverge at the edge, for comparison (blue dot-dashed). The edge result gives a valid description where the narrow-width approximation at NLO in α_s clearly fails. At the edge, power corrections $\mathcal{O}(\Gamma_{\tilde q}/m_{\tilde q})$ are missing. Going away from the edge, further power corrections of $\mathcal{O}(\Delta/m_{\tilde q}^2)$ arise, eventually become dominant, and destroy the validity of the edge description. For large width (upper plot in Fig. 5), missing power corrections are sizeable, as can be expected, such that there is no overlap region where the bulk/tail and edge results properly match. For medium width (middle plots in Fig. 5), the results for the three regions agree reasonably well if Δ is a few times $m_{\tilde q}\Gamma_{\tilde q}$. This is where the different approximations should be matched, since power corrections in the edge of the form $\Delta/m_{\tilde q}^2$ and logarithmically enhanced terms in the bulk/tail (see (2)) are both subdominant. The matching of the bulk/tail and the edge results improves with decreasing width as can be seen by comparing the upper and the lower plots in Fig. 5. However, for decreasing width, the logarithms of $m_{\tilde q}/\Gamma_{\tilde q}$ in the edge result increase and resummation of these logarithms becomes mandatory for an extremely small width. The onset of the unphysical behavior of the unresummed edge result can be seen close to the edge in the lower plot of Fig. 5.

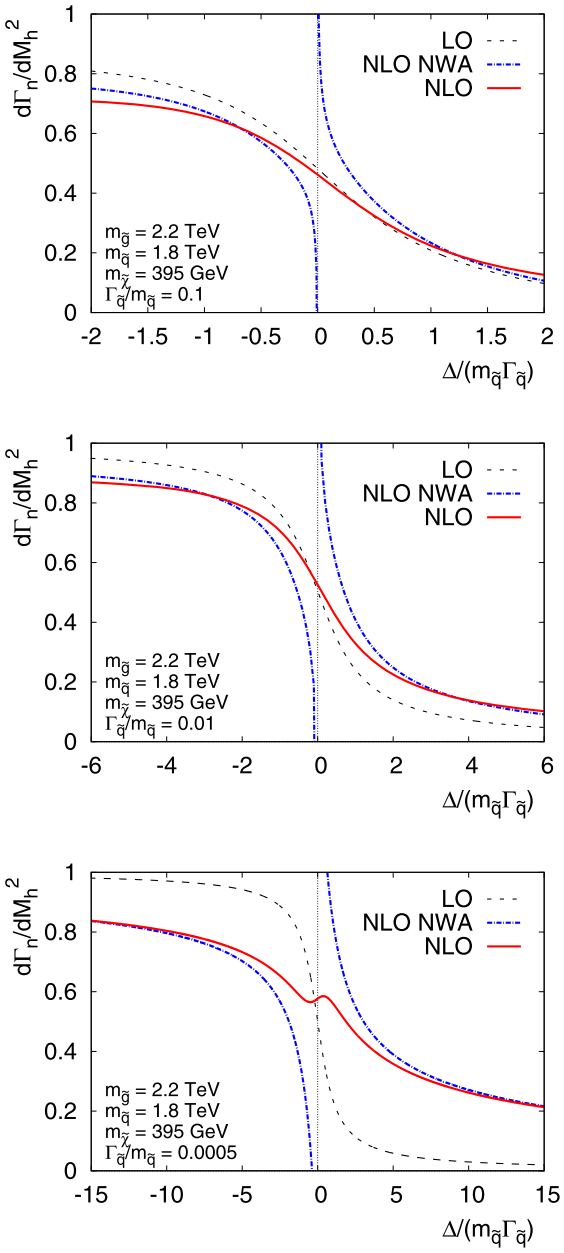

Fig. 5. Differential width as a function of the distance to the edge for the benchmark scenario A: $m_{\tilde{g}} = 2.2$ TeV, $m_{\tilde{q}} = 1.8$ TeV, $m_{\tilde{\chi}} = 395$ GeV, $\chi > 0$. As in Fig. 4, we normalize the differential width to the constant LO bulk region result in the narrow-width approximation. Shown are (black dashed) the full LO result in α_s (including all power corrections in $\Gamma_{\tilde{q}}/m_{\tilde{q}}$), (red solid) the NLO QCD corrections added, which is our main result, and (blue dot-dashed) the full LO result plus the NLO QCD corrections in the narrow-width approximation in the bulk and in the tail region. From top to bottom the plots refer to three different choices of the width: $\Gamma_{\tilde{q}}/m_{\tilde{q}} = 0.1$ (top), $\Gamma_{\tilde{q}}/m_{\tilde{q}} = 0.01$ (middle), $\Gamma_{\tilde{q}}/m_{\tilde{q}} = 0.0005$ (bottom). (For interpretation of the references to color in this figure, the reader is referred to the web version of this article.)

4. Conclusion

Kinematic edges of cascade decays of new particles produced in high-energy collisions may provide important constraints on the particle masses. Depending on the experimental resolution an accurate treatment of finite-width and higher-order radiative effects is required. In this work we performed a next-to-leading order calculation in the two small quantities α_s and $\Gamma_{\tilde{q}}/m_{\tilde{q}}$ for the hadronic invariant mass distribution in the vicinity of the kinematic edge of the gluino cascade decay $\tilde{g} \to q\bar{q}\tilde{\chi}$ through a squark resonance, based on a systematic expansion in $\Gamma_{\tilde{q}}/m_{\tilde{q}}$.

At NLO it is of course technically possible to perform a standard one-loop computation in the complex mass scheme, as was done for the electromagnetic correction to the decay $\tilde{\chi}_2^0 \to \ell\bar{\ell}\tilde{\chi}_1^0$ through a slepton resonance [12]. The approach discussed here is nevertheless interesting, since the separation into hard, collinear and soft contributions does not only simplify the calculation, but also elucidates the process-dependent and universal features of distributions in the edge region. We then find that these are described in terms of on-shell decay matrix elements, universal jet functions and a soft function that depends only on the resonance propagator and soft Wilson lines, one for each colored particle involved.

For very narrow resonances the perturbative approximation breaks down due to large width logarithms, a situation that becomes relevant only for exquisite experimental resolution. The factorization structure discussed here makes it clear that these logarithms can be summed with the help of renormalization group equations for the hard and jet functions. We hope to return to this in a future publication.

Acknowledgements

The work of M.B. has been supported in part by the Bundesministerium für Bildung und Forschung (BMBF) under project no. 05H15W0CAA. L.J. was partially supported by the DFG contract STU 615/1-1, and M.U. is partially supported by the STFC grant ST/L000385/1 and her research is funded by a Royal Society Dorothy Hodgkin Research Fellowship.

References

[1] I. Hinchliffe, F.E. Paige, M.D. Shapiro, J. Soderqvist, W. Yao, Precision SUSY measurements at CERN LHC, Phys. Rev. D 55 (1997) 5520–5540, arXiv:hep-ph/9610544.
[2] B.C. Allanach, C.G. Lester, M.A. Parker, B.R. Webber, Measuring sparticle masses in nonuniversal string inspired models at the LHC, J. High Energy Phys. 09 (2000) 004, arXiv:hep-ph/0007009.
[3] R. Horsky, M. Krämer, A. Mück, P.M. Zerwas, Squark cascade decays to charginos/neutralinos: gluon radiation, Phys. Rev. D 78 (2008) 035004, arXiv:0803.2603.
[4] C.W. Bauer, S. Fleming, D. Pirjol, I.W. Stewart, An effective field theory for collinear and soft gluons: heavy to light decays, Phys. Rev. D 63 (2001) 114020, arXiv:hep-ph/0011336.
[5] M. Beneke, A.P. Chapovsky, M. Diehl, T. Feldmann, Soft collinear effective theory and heavy to light currents beyond leading power, Nucl. Phys. B 643 (2002) 431–476, arXiv:hep-ph/0206152.
[6] M. Beneke, A.P. Chapovsky, A. Signer, G. Zanderighi, Effective theory approach to unstable particle production, Phys. Rev. Lett. 93 (2004) 011602, arXiv:hep-ph/0312331; Nucl. Phys. B 686 (2004) 205–247, arXiv:hep-ph/0401002.
[7] M. Beneke, V.A. Smirnov, Asymptotic expansion of Feynman integrals near threshold, Nucl. Phys. B 522 (1998) 321–344, arXiv:hep-ph/9711391.
[8] M. Beneke, Unstable-particle effective field theory, Nucl. Phys. B, Proc. Suppl. 261–262 (2015) 218–231, arXiv:1501.07370.
[9] M. Beneke, L. Jenniches, A. Mück, M. Ubiali, in preparation.
[10] W. Beenakker, R. Höpker, P. Zerwas, SUSY QCD decays of squarks and gluinos, Phys. Lett. B 378 (1996) 159–166, arXiv:hep-ph/9602378.
[11] ATLAS Collaboration, G. Aad, et al., Summary of the searches for squarks and gluinos using $\sqrt{s} = 8$ TeV pp collisions with the ATLAS experiment at the LHC, J. High Energy Phys. 10 (2015) 054, arXiv:1507.05525.
[12] M. Drees, W. Hollik, Q. Xu, One-loop calculations of the decay of the next-to-lightest neutralino in the MSSM, J. High Energy Phys. 02 (2007) 032, arXiv:hep-ph/0610267.